AIAA 94-0605

Ice Accretion on Aircraft Wings with Thermodynamic Effects

P. Tran, M.T. Brahimi, I. Paraschivoiu
Department of Mechanical Engineering
École Polytechnique de Montréal
Québec, Canada

A. Pueyo
Institute of Aerospace Studies
University of Toronto
Toronto, Canada

F. Tezok
Advanced Aerodynamics
Bombardier Inc./Canadair
Dorval, Québec, Canada

32nd Aerospace Sciences Meeting & Exhibit

January 10-13, 1994 / Reno, NV

ICE ACCRETION ON AIRCRAFT WINGS WITH THERMODYNAMIC EFFECTS

P. Tran*, M.T. Brahimi†, I. Paraschivoiu‡
Department of Mechanical Engineering
Ecole Polytechnique de Montréal
C.P. 6079, Succ. A, Montréal
P.Q., Canada, H3C 3A7

A. Pueyo*
Institute of Aerospace Studies
University of Toronto

F. Tezok§
Advanced Aerodynamics, Bombardier Inc./Canadair
Dorval, Québec, Canada

Abstract

The purpose of this paper is to present a computer code to predict ice shape that forms on aircraft for both rime and glaze ice conditions by analyzing the thermodynamic process involved during ice formation. The method used to determine the origin of the sweep and then the output number of impacts for each panel is based on the calculation of the stagnation point from which the calculation started. The thermodynamic characteristics of the freezing process of the incoming liquid water striking the iced wing is presented by considering the mass and energy balance on the wing surface where the ambient temperature is critical in determining the type of surface involved: dry, wet or liquid. Results using the present code to simulate ice deposit on NACA 0012 yield ice shapes that are in good agreement with numerical and experimental data.

Nomenclature

C_D = drag coefficient
c_f = skin-friction coefficient
c_g = specific heat capacity of ice, J/kgK
c_p = specific heat capacity of air, J/kgK
c_w = specific heat capacity of water, J/kgK
e = internal energy, J/kg
f = freezing fraction
$\vec{g}$ = gravitational acceleration vector, m/s^2
h = enthalpy, J/kg
h_c = convective heat transfer coefficient, W/m^2K
k_s = roughness height, m
L_e = latent heat of vaporization, J/kg
L_f = latent heat of fusion, J/kg
L_s = latent heat of sublimation, J/kg
LWC = liquid water content, kg/m^3
P_r = Prandtl number
$\dot{m}$ = mass flow rate, kg/s
$\dot{Q}$ = heat flux, J/s
R_e = Reynolds number
S = surface, m^2
St = Stanton number
St_k = roughness Stanton number
R_{ek} = local Reynolds number
T_o = reference temperature, K
T_s = surface temperature, K
V = velocity vector, m/s
$\dot{W}$ = power, J/s
ϑ = volume, m^3
δ = boundary layer thickness, m
η = collection efficiency
θ = momentum thickness, m
μ = dynamic viscosity, kg/ms
ν = kinematic viscosity, m^2/s
ρ = density, kg/m^3

1. Introduction

The formation of ice on aircraft components such as wings, control surfaces and engine intakes, occurs when the aircraft flies at a level where the temperature is at, or below freezing point and hits supercooled water droplets. Results from wind tunnel and flight icing tests indicate that the presence of ice accretion on unprotected aircraft components can lead to a number of aerodynamic degradation problems and consequently is a major problem of safety as indicated by many authors[1-4]. The most severe penalties encountered deal with decreased maximum lift, increased drag, decreased stall angle, changes in the pressure distribution, early boundary-layer transition, increased stall speed and reduced controllability. To overcome these penalties, various practical methods have been used to remove or prevent accumulation of ice on aircraft surfaces using deicing/anti-icing procedures. However, failure of protection systems and presence of residual ice accretion still produce a loss in the efficiency of aircraft. These problems, along with the number of icing-related accidents, have stimulated a new effort for research on aircraft icing. Among this

*PhD Student.
†Research Associate, Member AIAA.
‡Bombardier Chair Professor, Member AIAA.
§Advanced Aerodynamic Staff.

research, two important specialists' meeting have been organized in 1991, in Toulouse (France) by the Advisory Group for Aerospace Research and Development (AGARD)[5], and in 1993 in Montreal (Canada) by the J.-A. Bombardier Aeronautical Chair group[6]. Both meetings concluded that one of the most important steps that needs to be taken is to understand the physical processes of ice accretion. Surface roughness, boundary-layer transition, separated flow at the stall and post-stall angle, local heat transfer and collection efficiency are the major parameters that should be considered for a realistic understanding of ice accretion mechanisms[2,7].

In previous study, the Bombardier Aeronautical Chair group developed a 2-D ice accretion computer code which was extended to a 3-D inviscid code to predict rime ice shapes[8]. This code was then matched with a boundary layer calculation code to take into account the viscous effects (INTERICE code)[9]. Although this code predicts well rime ice accretions, the thermodynamic effects were neglected. For glaze ice conditions, which is formed at a temperature around 0 °C and high liquid water content, it is necessary to take thermodynamic analysis into account since the behaviour of unfrozen surface water has a direct influence on ice accretion mechanisms. The present work details the progress in the development of numerical code "THERMICE" that predict rime as well as glaze ice accumulations on aircraft wings.

2. Mechanism of aircraft icing

Aircraft can experience icing in temperatures ranging from 0 °C to -40 °C, however icing is usually restricted to the lower 30,000 feet of the troposphere (300 to 30,000 feet)[10,11]. The more dangerous types of ice are encountered in dense clouds, composed of heavy accumulation of large water droplets. When a droplet hits aircraft surfaces it begins to freeze immediately, however, as it freezes, heat is released so that its temperature rises until it reaches 0 °C. As this temperature is reached, freezing upon impact stops while the remaining liquid fraction of the droplet starts to run back along wing surface or along existing ice and freezes downstream. The rate of heat loss from the aircraft surfaces is such that some or all of the droplets are frozen before they can run off the body. The amount and the shape of ice accretion collected depend mainly on the liquid water content, the temperature, the airspeed, the droplet size and the surface roughness. Two basic types of ice can be formed, the rime ice, if all the impinging water droplets freeze upon impact, or glaze ice deposit if only a fraction of the water droplets freeze while the remainder run back and freeze downstream. Rime ice is a dry, opaque and milky white ice deposit which usually occurs at low airspeed, cold temperature and low liquid water content. It is characterized by the instantaneous freezing of small supercooled water droplets as soon as they reach and hit the surface of the aircraft without spreading from the point of impact trapping the air within the ice structure. In contrast, glaze ice (or clear ice) is a wet growth ice formed from the low freezing of large supercooled droplets at a warmer temperature (near freezing) and a higher liquid water content. It has a density closer to that of the cloud water indicating the wet nature of its formation. It is a heavy coating of glassy ice which spreads over the wing, has a clear appearance and where only a small part of the supercooled water droplets freezes on impact. This process produce double horned, beak or rounded glaze ice shapes.

3. Simulation of ice accretion

The computational procedure for ice accretion calculation is an iterative process where the flowfield influences the ice formation which, in turn, changes the flowfield. The shape of ice which will be formed is changed by successive accretion layers and is influenced by liquid water content (*LWC*), catch distribution, droplet diameter, temperature, free stream velocity, surface roughness and wing geometry. The overall ice simulation problem involves four main steps, these are: the flowfield calculation by a panel method, the particle trajectory calculation, the thermodynamic analysis and the ice accretion calculation. The main objective of ice simulation is the calculation of the impingement of the particles on the wing which involves the computation of the droplet trajectory through the local flowfield. A time stepping procedure is used with successive thin ice layers followed by a new flowfield and droplet impingement recalculations.

Trajectory calculation

The basic equation relating droplet trajectories is derived from Newton's law. In this equation, we take into account the buoyancy, gravity and drag forces[8]. The main objective of the droplet trajectory calculations is the simulation of the motion of droplets which impinge on the wing. The computation of these droplet trajectories is considered as the most time-consuming step since thousands of individual particles must be followed through their entire path. The droplet trajectory is calculated by integrating the droplet equation of motion over many time steps and an efficient scan procedure of the frontal surface of the wing permits the calculation of the flux of water impinging on each panel forming the surface. The initial droplet position is determined and its new position is recalculated after a time interval Δt. The amount of water that impinges on the wing depends on the normal surface of the wing to the freestream direction S_f, the freestream velocity $\vec{V}_\infty$ and the liquid water content *LWC*. Having determined the droplet impact points, the ice thickness at each point on the wing surface can be determined and then the geometry is updated. The method is based on the calculation of the stagnation point from which we determine the origin of the sweep and then the output number of impacts for each panel[12].

To calculate the droplet trajectories, we assume that the volume of the droplet remains constant throughout the entire process. Although the droplet may or may not keep

its spherical shape the droplet density ρ_d remains constant throughout the whole path, the initial droplet velocity is equal to the freestream velocity $\vec{V}_\infty$, the droplets are much smaller than the body considered so that they do not affect the velocity field. The equation of motion of the droplet is given by

$$m_d\vec{a}_d = (\rho_d - \rho_a)\vartheta\vec{g} + \frac{1}{2}\rho_a S C_D|\vec{U} - \vec{V}_d|(\vec{U} - \vec{V}_d) \qquad (1)$$

where m_d and $\vec{a}_d$ are the mass and the acceleration of the droplet, ρ_a and ρ_d the densities of air and water, ϑ the volume of the droplet, $\vec{U}$ and $\vec{V}_d$ the velocity vectors of the fluid and the droplet, S the area normal to the freestream direction and C_D represents the drag coefficient of the droplet. If the air velocity at a point $\vec{r}_d$ is $\vec{V}_a$, then equation (1) becomes

$$\frac{d^2\vec{r}_d}{dt^2} + \frac{C_D R_e}{24}\frac{1}{K_A}\frac{d\vec{r}_d}{dt} = K_G + \frac{C_D R_e}{24}\frac{1}{K_A}\vec{V}_a \qquad (2)$$

where $K_G = \frac{(\rho_d - \rho_a)}{\rho_d}g$ and $K_A = \frac{\rho_d D_d^2}{18\mu_a}$. Any deviation of the droplet from spherical shape is included in the drag coefficient. This deformation can be included in the modified drag coefficient $(C_D R_e/24)$ which depends only on the Reynolds number. It is given by Gunn and Kinzer[13].

$$\frac{C_D R_e}{24} = 1.699 \times 10^{-5}(R_e)^{1.92} \qquad (3)$$

The maximum amount of water that impinges on the wing depends on several parameters. The major parameters are S_f, the total frontal area of the wing to the freestream direction, the freestream velocity $\vec{V}_\infty$ and the liquid water content LWC. The true mass flow rate that impinges on the wing is lower because the droplets have tendency to follow the streamlines sweeping past the obstacle. The water mass flow rate that impinges on the wing is then given by

$$\dot{m}_{im} = \eta V_\infty S_f LWC \qquad (4)$$

where η, the total collection efficiency, is the ratio between the area at the release plane, between the upper and lower limit trajectories, and the maximum projected frontal area of the wing. This coefficient depends on several parameters including the shape and maximum thickness of the cross section of the wing, flight speed, angle of attack, droplet size, ambient temperature and pressure.

Impact point calculation

Three aerodynamic modules for determining the droplet trajectories have been developed: the mass flow calculation module, the trajectory calculation module and the impact calculation module. The objective is to sweep the domain in the y and z directions in order to get the impact points for each panel[12]. The method is based on the calculation of the stagnation point from which we determine the origin of the sweep and then the output number of impacts for each panel as shown in Fig. 1. During the sweep in both directions, the second module is needed to solve the droplet equation of motion. After determining the K_A and K_G coefficients, the location of the initial droplet and the velocity at a point P are calculated then a new location and velocity are calculated while a test on impact points gives whether the droplet hits the body or is outside.

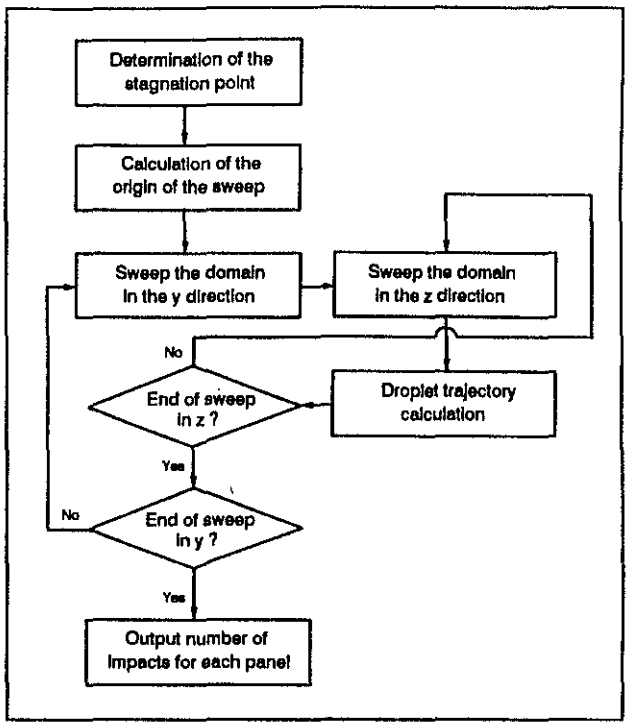

Fig. 1. Flowchart of the sweep module

In figure 2,an example of the order followed for sweep in y and z directions is presented. Once we get the first droplet which hits the body at the stagnation point, we sweep in the z direction for each value of y. The sweep ends whenever we find that a droplet does not hit the body (droplets number 9, 22, 36, 13, 26 of in Fig. 2.a). In the y direction the sweep ends when the droplet for any y position does not hit the body (droplet number 65 in Fig. 2.a). For high resolution a sub-sweep may be used as shown by Fig. 2.b. To calculate the impact of droplets we have to determine if there is intersection between a given trajectory segment and every triangular panel. If a droplet is moving from a point of (x'_d, y'_d, z'_d) coordinates to a point of (x_d, y_d, z_d) coordinates, then the trajectory can be written in parametric form as

$$x = x'_d + t_0(x_d - x'_d) \qquad (5)$$
$$y = y'_d + t_0(y_d - y'_d) \qquad (6)$$
$$z = z'_d + t_0(z_d - z'_d) \qquad (7)$$

where t_0 is a geometric parameter. Points which belong to the trajectory curve from x_d to x'_d must have $0 \le t_0 \le 1$. For a panel defined by the nodes x_1, x_2, x_3 the parametric equation can be written as

$$x = x_3 + t_1(x_1 - x_3) + t_2(x_2 - x_3) \quad (8)$$

$$y = y_3 + t_1(y_1 - y_3) + t_2(y_2 - y_3) \quad (9)$$

$$z = z_3 + t_1(z_1 - z_3) + t_2(z_2 - z_3) \quad (10)$$

For each point belonging to the panel we must have $0 \leq t_1 \leq 1$, $0 \leq t_2 \leq 1$ and $(t_1 + t_2) \leq 1$. If none of the panels have intersection with droplet segment studied, then we go on to the next segment until we find that the droplet hits or is outside the body surface.

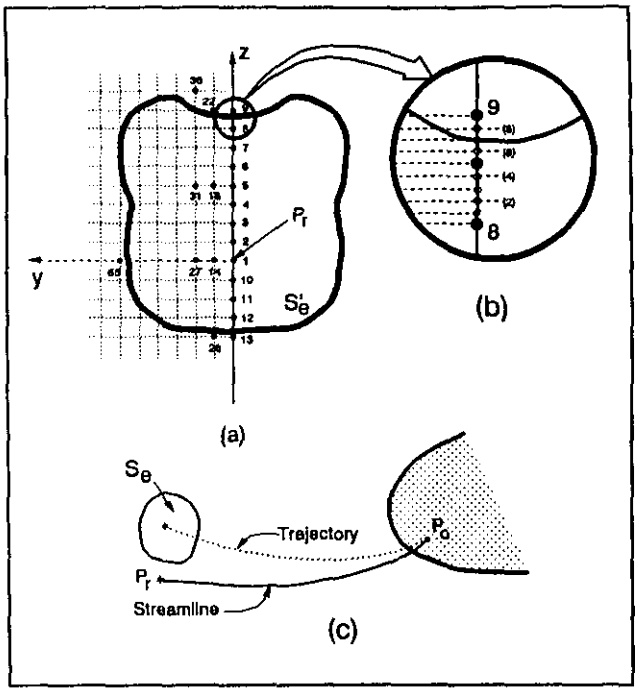

Fig. 2. Impact calculation and procedure for the sweep

4. Thermodynamic analysis

In the present paper, the thermodynamic characteristics of the freezing process of the incoming liquid water striking an iced wing is presented by considering the mass and energy balance on the wing surface. As previously stated, the incoming liquid water striking the wing surface may not automatically freezes on impact as in the case of rime ice accumulation but it may leave a fraction of the liquid running back along the wing surface and freezes downstream due to the insufficient heat transfer. This process is strongly related to the mass and heat transfer, surface roughness, skin friction, etc... Based on the mass flux and heat balance, the freezing fraction of the incoming water droplets for a control volume can be calculated, and along with the droplet impingement computation, the amount and growth of ice formed on this control volume can be determined. The ambient temperature is critical in determining the type of surface involved: dry, wet or liquid, and therefore on the energy balance. For a temperature near the freezing point, almost the entire wing surface is liquid whereas for glaze ice conditions, the surface is almost entirely wet. For rime ice conditions the wing surface is mostly or entirely dry.

Mass balance

To take into account the freezing process on wing surface we include the thermodynamic analysis by applying the first law of thermodynamic to the mass and energy balance for a control volume (CV). The model developed is based on the work done by Messinger[14]. The mass and heat flux are used to calculate the mass flow rate of the water running back out of the CV. A schematic representation of mass flux for a control volume is given in Fig. 3.

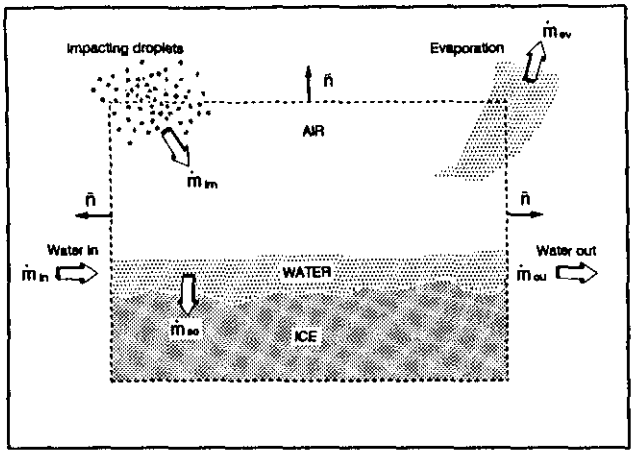

Fig. 3. Schematic representation of mass balance for a CV

In the present model we assume that the surface roughness is uniform and that only a fraction of the incoming liquid water freezes on impact while all the unfrozen part runs back along the wing surface and considered as an impinging water mass for downstream region. Three types of surface can arise: dry, wet and liquid surfaces. We obtain a dry surface when all the impinging water freezes on contact. In this case, a fraction of the ice can sublimate afterwards. If the heat absorption and dissipation are not sufficient to freeze all incoming water, we have a wet surface. A fraction of water freezes while the remainder runs back along the surface and into neighboring control volumes. In the case where no incoming water solidifies, we have a liquid surface. In that case, a fraction of the ice can evaporate afterwards. The continuity equation for the control volume in Fig. 3 is written as

$$\frac{d(m_s + m_l + m_v + m_a)}{dt} + \sum_{s,l,v,a} \int_S \rho \vec{V} \vec{n} dS = 0 \quad (11)$$

The subscripts s, l, v and a represent the different phases present in the control volume: solid water or ice, liquid water, vapor and air. The time derivatives of the mass of air, liquid water and vapor are equal to zero since we consider a steady flow and constant mass flow rates. Therefore the first term of equation (11) becomes

$$\frac{d(m_s + m_l + m_v + m_a)}{dt} = \frac{dm_s}{dt} = \dot{m}_{so} \quad (12)$$

The surface integral is equal to zero for air since the mass flux entering the volume is equal to the mass flux coming out of it. It is also equal to zero for solid water since it

does not cross the control volume boundaries. Since the properties are constant on each boundary of the control volume, we can write

$$\sum_{l,v} \int_S \rho \vec{V} \vec{n} dS = \dot{m}_{ou} - \dot{m}_{in} + \dot{m}_{va} - \dot{m}_{im} \quad (13)$$

Combining equations (12) and (13) the equation governing the mass balance for the control volume can be written as

$$\dot{m}_{im} + \dot{m}_{in} = \dot{m}_{va} + \dot{m}_{ou} + \dot{m}_{so} \quad (14)$$

where $\dot{m}_{im}$ is the mass flow rate of the impinging water, $\dot{m}_{in}$ is the mass flow rate of the water flow in the control volume (runback water from previous CV), $\dot{m}_{va}$ is the mass flow rate due to evaporation or sublimation, $\dot{m}_{ou}$ is the mass flow rate of the water flow out of the control volume (runback water to next CV) and $\dot{m}_{so}$ is the mass flow rate of the accumulated ice. The mass flow rate of the water flow out of the control volume due to evaporation/sublimation and due to freezing are determined from the energy balance equations.

The freezing fraction, f, defined as the fraction of incoming liquid water that freezes within the region of impingement should be equal to 1 ($f = 1$) for the rime ice since all the incoming liquid water is assumed to freeze. f can be computed from the following relation

$$f = \frac{\dot{m}_{so}}{\dot{m}_{im} + \dot{m}_{in}} \quad (15)$$

The mass flow rate of the water flow out of the control volume or runback water to the next control volume can be calculated using

$$\dot{m}_{ou} = (1 - f)(\dot{m}_{im} + \dot{m}_{in}) - \dot{m}_{va} \quad (16)$$

Energy balance

The impinging water due the impacting droplets along with the energy of water runback from previous control volume and the heat released by freezing water represent the energy flow into the control volume while the convection conduction, evaporation and the energy of water runback out represent the energy flow out of the control volume. From the first principle of thermodynamics we can write

$$\frac{d(E_s + E_l + E_v + E_a)}{dt} + \sum_{s,l,v,a} \int_S e\rho \vec{V} \vec{n} dS = \dot{Q} - \dot{W} \quad (17)$$

where $\dot{Q}$ and $\dot{W}$ represent respectively the heat flux and the power developed. The surface integral for solid water is equal zero since ice does not cross control volume boundaries. Since the only external heat source would be coming from a thermal deicing or anti-icing system, the $\dot{Q}$ term is also set to zero. The power needed to move the mass to and from the control volume is the only one developed by the system.

$$\frac{d(E_s + E_l + E_v + E_a)}{dt} + \sum_{l,v,a} \int_S \rho e \vec{V} \vec{n} dS = -\sum_{l,v,a} \int_S P \vec{V} \vec{n} dS \quad (18)$$

Using the relation for the enthalpy, $\rho h = \rho e + P$, we get

$$\frac{d(E_s + E_l + E_v + E_a)}{dt} + \sum_{l,v,a} \int_S \rho h \vec{V} \vec{n} dS = 0 \quad (19)$$

Since we have neglected any chemical reactions or mixing between air and water, the overall system is divided into two subsystems, one for air and one for water, where we have

$$\sum_{a} \int_S \rho h \vec{V} \vec{n} dS = \dot{Q}_1 - \dot{W}_1 \quad (20)$$

$$\frac{dE_s}{dt} + \sum_{l,v} \int_S \rho h \vec{V} \vec{n} dS = \dot{Q}_2 - \dot{W}_2 \quad (21)$$

$\dot{Q}_1 = -\dot{Q}_2$ and $\dot{W}_1 = -\dot{W}_2$. Since there is no work done between the two subsystems $\dot{W}_1 = \dot{W}_2 = 0$. In this thermodynamic analysis, we will consider two heat terms: heat gained by water from the air by friction $\dot{Q}_f$ and heat lost by water to air by convection $\dot{Q}_c$.

$$\dot{E}_{so} + \dot{H}_{va} + \dot{H}_{ou} + \dot{H}_{in} + \dot{H}_{im} = \dot{Q}_f - \dot{Q}_c \quad (22)$$

For the heat gained by friction we have[14]

$$\dot{Q}_f = h_c A r \frac{V_\infty^2}{2c_p} \quad (23)$$

where A is the panel area, h_c the convection coefficient and r is the recovery factor applying to kinetic heating.

$$r = 1 - (\frac{V}{V_\infty})^2 [1 - (P_r)^n] \quad (24)$$

V is the velocity at a given panel, $n = 1/2$ in laminar regime, $n = 1/3$ in turbulent regime and Pr, Prandtl's number, is defined as

$$P_r = \frac{\mu c_p}{k_a} \quad (25)$$

For the heat lost due to convection

$$\dot{Q}_c = h_c A (T_s - T_\infty) \quad (26)$$

Therefore, the net heat flux applied to the water subsystem is obtained by the difference between the two heat flux terms

$$\dot{Q} = h_c A \left[r \frac{V_\infty^2}{2c_p} - (T_s - T_\infty) \right] \quad (27)$$

Internal energy and enthalpy

Enthalpy and internal energy are calculated in relation to a given reference state. The chosen reference state is

Figure 4 shows the different processes involved in the control volume for the three types of surface: dry, wet and liquid respectively. It shows the various mass flux and enthalpy variations involved. In the case of a dry surface, liquid water enters the control volume at states H and I and then solidifies to state S. Then, a fraction of the ice sublimates to state V. In the case of a wet surface, liquid water enters the control volume at states H and I and a fraction is heated to a temperature T_o. A fraction solidifies to state S, another evaporates to state V and the rest runs back outside the volume. The surface reaches an equilibrium temperature of $T_s = T_o$. In the case of a liquid surface, all the incoming water is heated to a temperature $T_s > T_o$. A fraction evaporates to state V.

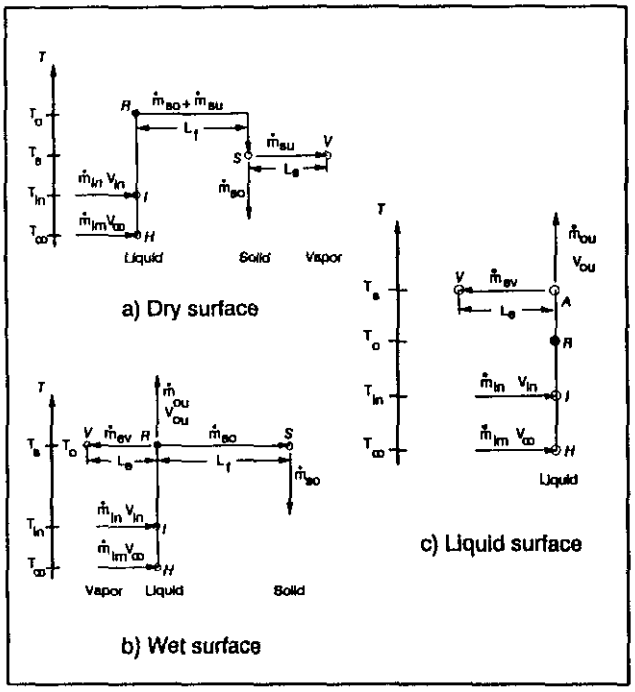

Fig. 4. Processes involved for different surface types

The internal energy for the three cases is

$$\dot{E}_{so} = \dot{m}_{so}|c_g(T_s - T_o) - L_f| \quad \text{for dry surface}$$

$$\dot{E}_{so} = -\dot{m}_{so}L_f \quad \text{for wet surface}$$

$$\dot{E}_{so} = 0 \quad \text{for liquid surface}$$

Two terms of enthalpy variation are coming into the control volume: the enthalpy associated with impinging water and with runback water entering the volume. These are calculated using the following relations

$$\dot{H}_{im} = \dot{m}_{im}\left[c_w(T_\infty - T_o) + \frac{V_\infty^2}{2}\right] \tag{28}$$

$$\dot{H}_{in} = \dot{m}_{in}c_w(T_{in} - T_o) \tag{29}$$

Depending on the type of surface considered, water can leave the volume by several ways and different enthalpy variations are associated with each one. For a dry surface, water can only leave by sublimation ($\dot{H}_{ou} = 0$), so the enthalpy variation terms is given by

$$\dot{H}_{su} = \dot{m}_{va}|L_s + c_g(T_s - T_o) - L_f| \tag{30}$$

L_s is the latent heat of sublimation, c_g is the specific heat capacity of ice and L_f is the latent heat of fusion and is equal to 333.3 kJ/kg.

For a wet surface, water can leave by evaporation or by running back to neighboring control volumes. With L_e the latent heat of evaporation the enthalpy variations involved are

$$\dot{H}_{ou} = \dot{m}_{ou}\frac{V_\infty^2}{2} \simeq 0 \tag{31}$$

$$\dot{H}_{ev} = \dot{m}_{va}L_e \tag{32}$$

Finally, in the case of a liquid surface, water can leave also by evaporation or by running back out of the volume, but we have to take into account the temperature change from T_o to T_s.

$$\dot{H}_{ou} = \dot{m}_{ou}c_w(T_s - T_o) \tag{33}$$

$$\dot{H}_{ev} = \dot{m}_{va}[L_e + c_w(T_s - T_o)] \tag{34}$$

MacArthur[15] gives a relation to calculate the mass flux that evaporates or sublimates as

$$\dot{m}_{va} = \frac{0.7}{c_p}h_c A\left[\frac{p_{v,s} - H_r p_{v,e}}{P_e}\right] \tag{35}$$

c_p is the specific heat capacity of air, $p_{v,s}$ is the saturation vapor pressure at the surface, H_r is the relative humidity, $p_{v,e}$ is the saturation vapor pressure of water in ambient air and P_e is the absolute pressure above the control volume, outside the boundary layer. The pressure for an isentropic process is given by

$$P_e = P_t\left[\frac{T_e}{T_t}\right]^{\gamma/(\gamma-1)} \tag{36}$$

where P_t is total pressure, T_t the total temperature and T_e the temperature outside the boundary layer. The saturation vapor pressure is calculated using[16]

$$p_v = 3386(0.0039 + 6.809610^{-6}T^2 + 3.557910^{-7}T^3) \tag{37}$$

$$T = 72 + 1.8(T_s - 273.15) \tag{38}$$

The thermodynamic analysis yields three equations (14), (22), (35) and four unknowns, T_s, $\dot{m}_{so}$, $\dot{m}_{ou}$ and $\dot{m}_{va}$.

The fourth equation is given by the type of surface involved, dry surface ($\dot{m}_{ou} = 0$), wet surface ($T_s = T_o$) or liquid surface ($\dot{m}_{so} = 0$).

Calculation of the heat transfer

The heat transfer coefficient have two relations one for the laminar region and one for turbulent region. For the laminar region the heat transfer coefficient is given by

$$h_{c,l} = 0.296 \frac{k_a}{\sqrt{\nu}} \left[u_e^{-2.88} \int_0^s u_e^{1.88} ds \right]^{-1/2} \quad (39)$$

where k_a is the thermal conductivity of the air and u_e is the surface velocity obtained by the flow field calculation. To determine the laminar-turbulent transition, we make use of Von Doenhoff criterion[17]

$$R_{ek} = \frac{u_k k_s}{\nu} \geq 600 \quad (40)$$

where k_s represents the roughness element height and u_k is the velocity at y = k_s. This velocity must be calculated to evaluate the local Reynolds number based on roughness element height. When R_{ek} exceeds 600, the boundary layer is assumed to be turbulent. The local velocity u_k is calculated from the following equation

$$\frac{u_k}{u_e} = \frac{2k_s}{\delta} - 2\left(\frac{k_s}{\delta}\right)^3 + \left(\frac{k_s}{\delta}\right)^4 + \frac{1}{6}\frac{\delta^2}{\nu}\frac{du_e}{ds}\frac{k_s}{\delta}\left(1 - \frac{k_s}{\delta}\right)^3 \quad (41)$$

To calculate the boundary layer thickness, δ, we have[12]

$$\delta = \frac{315}{37}\theta_l \quad (42)$$

Then from Thwaites[18] relation we get the following momentum thickness

$$\frac{\theta_l^2}{\nu} = \frac{0.45}{u_e^6} \int_0^s u_e^5 ds \quad (43)$$

The heat transfer coefficient for the turbulent region is obtained from the definition of Stanton number.

$$h_{c,t} = St \rho u_e c_p \quad (44)$$

$$St = \frac{c_f/2}{Pr_t + \frac{\sqrt{c_f/2}}{St_k}} \quad (45)$$

where Pr_t is the turbulent Prandtl number and is equal to 0.9 for air and St_k the roughness Stanton number

$$St_k = 1.156 \left[\frac{u_\tau k_s}{\nu}\right]^{-0.2} \quad (46)$$

where the shear velocity is

$$u_\tau = u_e \sqrt{\frac{c_f}{2}} \quad (47)$$

Finally, the skin friction coefficient is evaluated from

$$\frac{c_f}{2} = \frac{0.168}{[ln(864\frac{\theta_t}{k_s})]^2} \quad (48)$$

and the turbulent momentum thickness is

$$\theta_{t(s)} = \left[\frac{0.0156}{u_e^{4.11}} \int_{s'}^s u_e^{3.86} ds\right]^{0.8} + \theta_l s' \quad (49)$$

where s' represents the s value at the transition point.

5. Results and discussion

THERMICE has been tested in rime and glaze ice conditions and compared with experimental data and numerical results published by Olsen et al. [19] and Shin et al.[20]. All the test cases were performed for a mean equivolumetric diameter of 20 microns and an angle of attack of 4 degrees. Figure 5 shows the results for an ambiant temperature of -30.5 $°C$, an airspeed of 94 m/s, a liquid water content of 1.05 g/m^3 and an accumulation time of 6.2 minutes. The resulting ice shape obtained with THERMICE compares well, for both shape and amount of ice, with experimental data. Figure 6 shows a comparison between results calculated with THERMICE and results given by Shin et al.[20] in rime ice conditions. The ambiant temperature is set to -19.8 $°C$, the air velocity at 58 m/s, liquid water content equals 1.30 g/m^3 and for an accretion time of 8 minutes. Again, the calculated ice shape compares well with experimental data, particularly for the impingement limits on the upper and lower surface of the airfoil.

Having validated THERMICE in rime ice conditions, we have conducted some tests in glaze ice conditions. Figure 7 shows results obtained with the present method with a series of experiments conducted by Olsen et al.[19]. The test conditions are: ambiant temperature of -8 $°C$, airspeed of 58 m/s, liquid water content of 2.10 g/m^3 and accretion time of 5 minutes. We can observe that the horn is well predicted by THERMICE but the lower impingement limit and consequently the accumulated mass of ice is overestimated. Finally, we have tested THERMICE with the following icing conditions: temperature of -6.6 $°C$, airspeed of 94 m/s, LWC of 1.05 g/m^3 and an accretion time of 6.2 minutes. Figure 8 shows the resulting ice shape compared with experimental and numerical data obtained by Shin et al.[20]. The results obtained with THERMICE compare well with the numerical data but the experimental ice shape is not well reproduced. This is the weakness of icing codes to predict glaze ice shape. The present thermodynamic analysis neglects the microphysical factors involved in icing process such as bead formation and the effect of the angle of impact. To obtain such irregular shapes, we should increase the accuracy of our thermodynamic analysis by adding microphysical effects.

6. Conclusion

An icing code including thermodynamic effects has been developed. It predicts well ice accretion in rime ice conditions. However, for some glaze ice cases the predicted results do not agree well with experimental data. This may be due to some effects that are neglected in the present method. Hansman[7] has shown that the process of bead formation has a considerable influence on the resulting ice shape. Therefore, implementing a method which would take into account the bead formation and other microphysical factors would increase the accuracy of the method.

To increase the efficiency of the integration method, we plan to use an hybrid method: CRV method (Constant Relative Velocity) far from the body and we would switch to Runge-Kutta of the fourth order in the vicinity of the wing. The CRV method is much faster and therefore would save some computing time. The CRV method consists of assuming that the acceleration is constant on the trajectory segment, and using the equations for uniformly accelerated motion instead of integrating the droplet equation of motion.

Acknowledgements

This work was prepared in the context of J.-Armand Bombardier Aeronautical Chair. The authors would like to acknowledge the support provided by Advanced Aerodynamics Bombardier Inc., Canadair Group.

References

1. Brumby, R.E., *"The Effect of Wing Ice Contamination on Essential Flight Characteristics"*, AGARD-CP-496, 1991, pp. 2.1-2.4.

2. Mavriplis, F., *"Icing and Contamination of Aircraft Surfaces: Industry's Concerns"*, Proceedings of the First Bombardier International Workshop on Aircraft Icing and Boundary-Layer Stability and Transition, Montréal, Canada, September 20-21, 1993, pp. 51-55.

3. Bragg, M.B., *"Experimental Aerodynamic Characteristics of an NACA 0012 Airfoil with Simulated Glaze Ice"*, Journal of Aircraft, Vol. 25, No. 9, September 1988, pp. 849-854.

4. Potapczuk, M.G. and Reinmann, J.J., *"Icing Simulation: A Survey of Computer Models and Experimental Facilities"*, AGARD-CP-496, 1991, pp. 5.1-5.27.

5. *"Effects of Adverse Weather on Aerodynamics"*, AGARD Conference Proceedings CP-496, 1991.

6. *"Proceedings of the First Bombardier International Workshop on Aircraft Icing and Boundary-Layer Stability and Transition"*, Edited by I. Paraschivoiu, Montréal, Canada, September 20-21, 1993.

7. Hansman, R.J., *"Microphysical Factors Which Influence Ice Accretion"*, Proceedings of the First Bombardier International Workshop on Aircraft Icing and Boundary-Layer Stability and Transition, Montréal, Canada, September 20-21, 1993, pp. 86-103.

8. Tran, P., Brahimi, M.T. and Paraschivoiu, I., *"Effects of Ice Accretion on Aircraft Components"*, Final Report, prepared for Bombardier Inc./Canadair, C.D.T. Project C128, August 1992.

9. Paraschivoiu, I., Tran, P. and Brahimi, M.T., *"Prediction of Ice Accretion with Viscous Effects on Aircraft Wings"*, AIAA Paper 93-0027 (also AIAA Journal of Aircraft, in press).

10. Britton, R.K., *"Computer Simulation of Airfoil Icing Without Runback"*, AIAA Paper 91-0661.

11. Guffond, D., *"Le givrage des aéronefs"*, l'Aéronautique et l'Astronautique, No 148-149, 1991-3/4, pp. 51-54.

12. Pueyo, A., *"Simulation numérique de la formation de la glace pour des écoulements tridimensionnels"*, M.Sc.A. Thesis, Department of Mechanical Engineering, École Polytechnique de Montréal, July 1992.

13. Gunn, R. and Kinzer, G.D., *"The Terminal Velocity of Fall for Water Droplets in Stagnant Air"*, Journal of Meteorology, Vol. 6, August 1949.

14. Messinger, B.L., *"Equilibrium Temperature of an Unheated Icing Surface as a Function of Air Speed"*, Journal of the Aeronautical Sciences, January 1953.

15. MacArthur, C.D., Keller, J.L. and Luers, J.K., *"Mathematical Modeling of Ice Accretion on Airfoils"*, AIAA 20th Aerospace Sciences Meeting, January 11-14, 1982.

16. Asselin, M., Prud'homme, M. and Paraschivoiu, I., *"Analyse du mouvement des gouttelettes d'eau et formation de la glace en aéronautique"*, Département de Génie Mécanique, École Polytechnique de Montréal, Rapport final, Projet C.D.T. C089, Canadair, Août 1990.

17. Von Doenhoff, A.E. and Horton, E.A., *"A Low Speed Experimental Investigation of the Effect of Sandpaper Type of Roughness on Boundary-Layer Transition"*, NACA TN 3858, 1956.

18. Thwaites, B., *"Incompressible Aerodynamics"*, Clarendon Press, Oxford, 1960.

19. Olsen, W., Shaw, R. and Newton, J., *"Ice Shapes and the Resulting Drag Increase for NACA 0012 Airfoil"*, NASA Technical Memorandum 83556, 1984.

20. Shin, J., Berkowitz, B., Chen, H. and Cebeci, T., *"Prediction of Ice Shapes and their Effect on Airfoil Performance"*, AIAA Paper 91-0264.

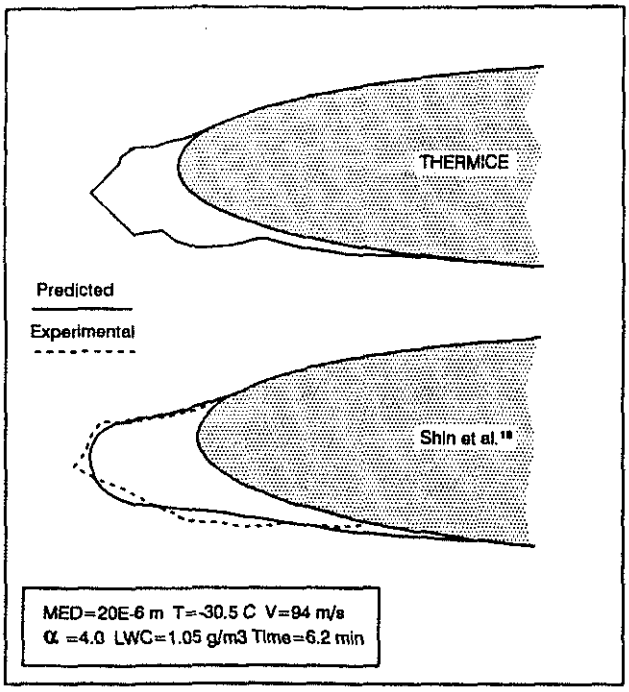

Fig. 5. Comparison of computed and experimental ice shapes in rime ice conditions (T = -30.5 C)

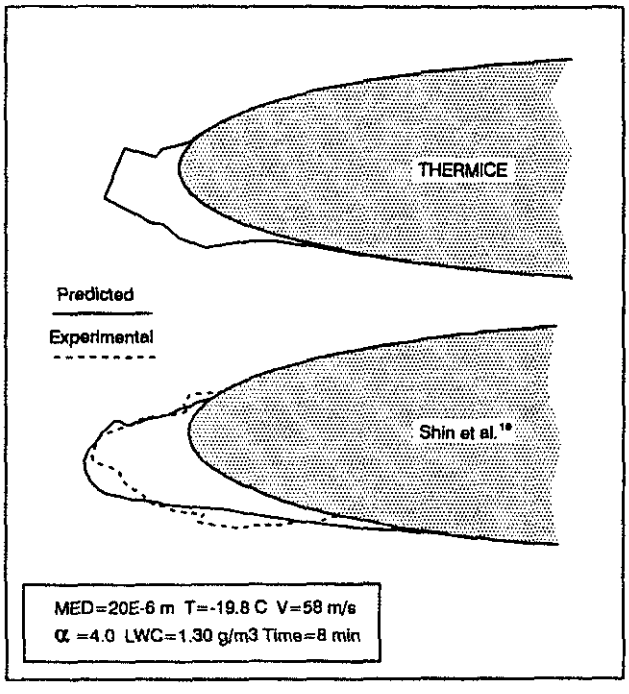

Fig. 6. Comparison of computed and experimental ice shapes in rime ice conditions (T = -19.8 C)

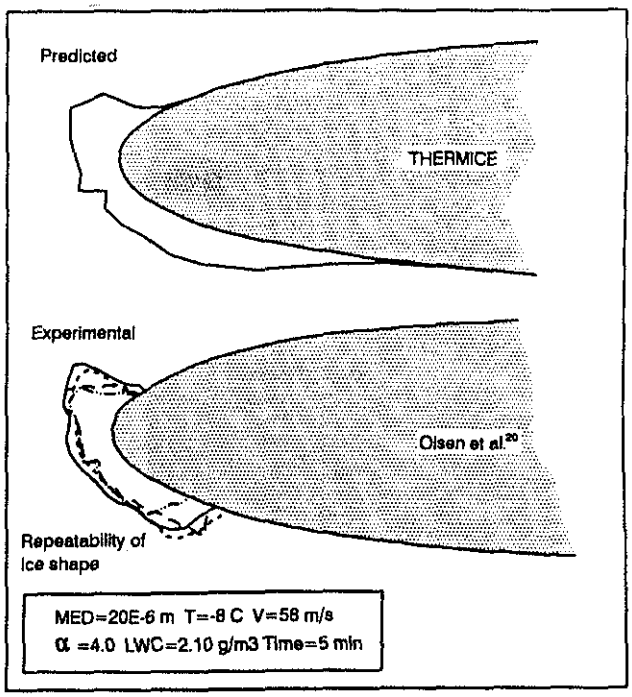

Fig. 7. Comparison of computed and experimental ice shapes in glaze ice conditions (T = -8 C)

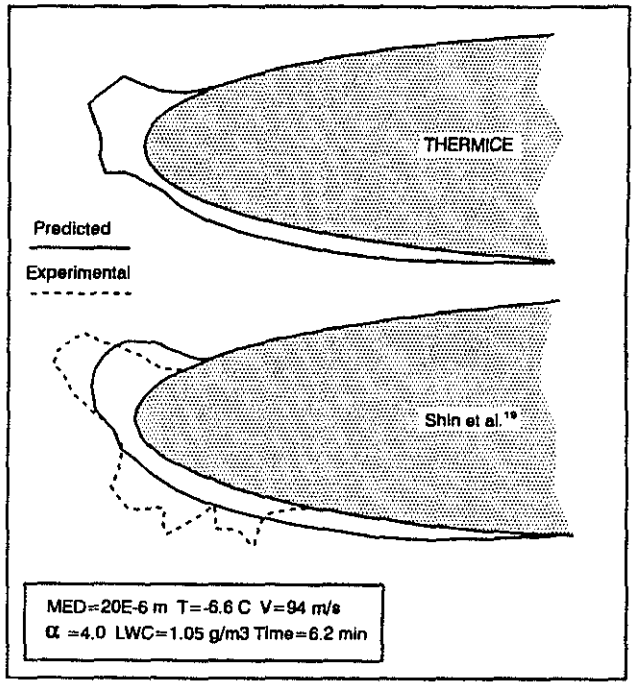

Fig. 8. Comparison of computed and experimental ice shapes in glaze ice conditions (T = -6.6 C)